

Provided for non-commercial research and education use.
Not for reproduction, distribution or commercial use.



This article appeared in a journal published by Elsevier. The attached copy is furnished to the author for internal non-commercial research and education use, including for instruction at the authors institution and sharing with colleagues.

Other uses, including reproduction and distribution, or selling or licensing copies, or posting to personal, institutional or third party websites are prohibited.

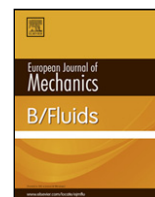
In most cases authors are permitted to post their version of the article (e.g. in Word or Tex form) to their personal website or institutional repository. Authors requiring further information regarding Elsevier's archiving and manuscript policies are encouraged to visit:

<http://www.elsevier.com/copyright>



Contents lists available at ScienceDirect

European Journal of Mechanics B/Fluids

journal homepage: www.elsevier.com/locate/ejmflu

The kinematics and stability of solitary and cnoidal wave solutions of the Serre equations

John D. Carter^{a,*}, Rodrigo Cienfuegos^b

^a *Mathematics Department, Seattle University, 901 12th Avenue, Seattle, WA 98122, United States*

^b *Departamento de Ingeniería Hidráulica y Ambiental, Pontificia Universidad Católica de Chile, Av. Vicuña Mackenna 4860-Macul, Santiago de Chile, Chile*

ARTICLE INFO

Article history:

Received 1 August 2010

Received in revised form

1 December 2010

Accepted 3 December 2010

Available online 16 December 2010

Keywords:

Serre

Stability

Kinematics

Nonlinear

ABSTRACT

The Serre equations are a pair of strongly nonlinear, weakly dispersive, Boussinesq-type partial differential equations. They model the evolution of the surface elevation and the depth-averaged horizontal velocity of an inviscid, irrotational, incompressible, shallow fluid. They admit a three-parameter family of cnoidal wave solutions with improved kinematics when compared to KdV theory. We examine their linear stability and establish that waves with sufficiently small amplitude/steepness are stable while waves with sufficiently large amplitude/steepness are unstable.

© 2010 Elsevier Masson SAS. All rights reserved.

1. Introduction

The evolution of gravity waves on the surface of an inviscid, incompressible fluid can be modeled by the Euler equations or by means of potential flow theory under the additional constraint of irrotationality. For many applications in the nearshore zone, it is customary to derive approximate versions of the Euler or potential flow systems by using a small-parameter perturbation procedure as done by, for example [1]. Generally, the derivation of these simplified models, which are known as Boussinesq-type models [2], requires the introduction of the following standard dimensionless parameters

$$\epsilon = \frac{H}{h_0} \quad \text{and} \quad \delta = \frac{h_0}{\lambda}. \quad (1)$$

Here H , h_0 and λ are positive constants representing a typical wave height, the mean depth of the fluid, and a typical wavelength in the horizontal dimension, respectively. Fig. 1 contains a plot of the physical system and graphically defines important parameters and variables. The parameter ϵ measures the strength of nonlinearity and δ is a measure of the dispersion. The wave steepness, Λ , and the Ursell number, U_r , are defined in terms of ϵ and δ via the following

expressions

$$\Lambda = \epsilon \delta = \frac{H}{\lambda} \quad \text{and} \quad U_r = \frac{\epsilon}{\delta^2} = \frac{H \lambda^2}{h_0^3}. \quad (2)$$

The Ursell number measures the relative importance of nonlinear effects in comparison to dispersion and can be used to distinguish between different types of approximations describing wave propagation. For waves of finite amplitude,

1. $U_r \gg 1$ corresponds to the nondispersive nonlinear approximation [3],
2. $U_r \sim O(1)$ corresponds to the weakly dispersive nonlinear approximation [2,4,5], and
3. $U_r \ll 1$ corresponds to the linear dispersive approximation [6].

Although Boussinesq-type equations are more appropriate for $U_r \sim O(1)$ and moderately nonlinear waves, they should in principle limit to the dispersionless nonlinear shallow water model as $U_r \rightarrow \infty$.

The Korteweg–de Vries (KdV) equation is the classic nonlinear model of long waves in shallow water [4]. It is derived from the Euler system by assuming $\delta^2 \sim \epsilon \ll 1$ (i.e. $U_r \sim 1$). It has been well studied both mathematically (see, for example, [7–9]) and experimentally (see, for example, [10–12]). Benjamin [13] established that the solitary wave solution of KdV is stable regardless of amplitude. Bottman and Deconinck [14] prove that all KdV cnoidal waves are stable regardless of their amplitude and/or steepness. These results are counter intuitive because we expect that physical waves with sufficiently large amplitude are unstable.

* Corresponding author.

E-mail addresses: carterj1@seattleu.edu (J.D. Carter), racienfu@ing.puc.cl (R. Cienfuegos).

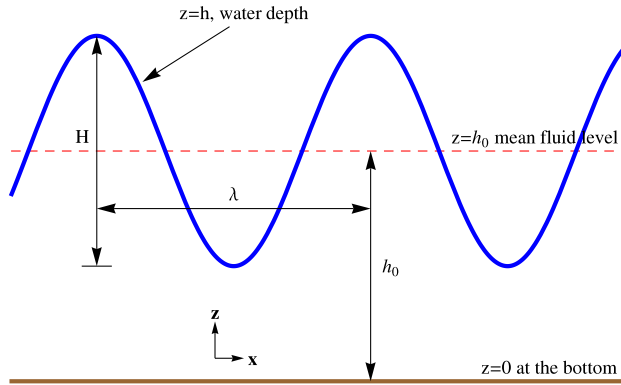


Fig. 1. The physical system and parameters under consideration.

However, we must remember that KdV is an approximation to the Euler system and is only a valid model for small amplitude, fairly long waves.

Recently, much progress has been made in providing a solid theoretical background for the family of Boussinesq-type wave equations both from a mathematical standpoint and for engineering applications. Bona et al. [15] provide a thorough mathematical review of many higher-order Boussinesq-type models for small amplitude, weakly dispersive waves. Chen et al. [16] establish that all cnoidal and solitary wave solutions to some of these Boussinesq systems are stable regardless of amplitude and/or steepness. (They also establish that these solutions are unstable with respect to two-dimensional perturbations. However in our current paper, we only consider the one-dimensional problem.) Madsen and Schäffer [1] present several higher-order models which have been, to some extent, used in engineering practice.

When no assumption is made on the order of magnitude of ϵ (i.e. assuming that $\epsilon \sim O(1)$), large amplitude waves propagating in shallow water can be described. The first strongly nonlinear, weakly dispersive set of Boussinesq-type equations was derived by Serre [5,17]. Several years later, Su and Gardner [18] and Green and Naghdi [19] re-derived the Serre equations using different methods. In the literature, the equations are referred to as both the Serre equations and the Green and Naghdi equations. The Serre equations are obtained by depth-averaging the Euler system and truncating the resulting set of equations at $O(\delta^4)$ without making any assumptions on the order of ϵ . This “full nonlinearity” makes the Serre equations ideal for studying large amplitude or nearly breaking waves in the nearshore zone. A formal derivation of the Serre equations using series expansion on small perturbation parameters is presented by Barthélemy [20] for horizontal bottoms and by Cienfuegos et al. [21] for non-horizontal bottoms. Recently, Dias and Milewski [22] derived an extended set of the Serre equations including the effect of surface tension and a variable level to define the velocity field. Li [23,24] established that small amplitude solitary wave solutions of the Serre equations are linearly stable.

The accuracy of the Serre equations in describing strongly nonlinear shallow water waves has been confirmed by multiple comparisons between numerical simulations and physical experiments including solitary waves propagating over a step [25], solitary waves shoaling over different slopes [20,26], and regular wave shoaling and breaking over uniform beach slopes where extra terms had to be incorporated to account for energy dissipation [27]. Guizien and Barthélemy [28] generated solitary waves in a flume with minimal trailing waves by using the solitary wave solution to the Serre equations. Finally, the theoretical analysis of Lannes and Bonneton [29] shows that the Serre equations constitute a relevant

system to model highly nonlinear waves propagating in shallow waters.

In this paper, we investigate additional properties of the Serre equations related to the existence of closed-form periodic solutions and their stability. Section 2 contains some mathematical properties of the Serre equations including a three-parameter family of periodic solutions. The accuracy and relevance of the Serre solitary and cnoidal solutions are investigated in Section 3. Section 4 contains our main result: waves with sufficiently small amplitude/steepness are stable while waves with sufficiently large amplitude/steepness are unstable.

2. The Serre equations

The dimensional Serre equations that describe water waves propagating on a horizontal bottom are [20],

$$h_t + (hu)_x = 0, \quad (3a)$$

$$u_t + uu_x + gh_x - \frac{1}{3h} \left(h^3 (u_{xt} + uu_{xx} - (u_x)^2) \right)_x = 0, \quad (3b)$$

where $u = u(x, t)$ is the depth-averaged horizontal velocity of the fluid, $h = h(x, t)$ is the water depth, and g is the acceleration due to gravity. We focus this pair of equations with periodic boundary conditions, though we also comment on the solitary wave limit.

The Serre equations admit the following conservation laws

$$\partial_t (h) + \partial_x (hu) = 0, \quad (4a)$$

$$\begin{aligned} \partial_t (hu) + \partial_x \left(\frac{1}{2} gh^2 + hu^2 - \frac{1}{3} h^3 u_{xt} \right. \\ \left. + \frac{1}{3} h^3 u_x^2 - \frac{1}{3} h^3 uu_{xx} \right) = 0, \end{aligned} \quad (4b)$$

$$\begin{aligned} \partial_t \left(\frac{1}{2} h \left(gh + u^2 + \frac{1}{3} h^2 u_x^2 \right) \right) + \partial_x \left(hu \left(gh + \frac{1}{2} u^2 \right. \right. \\ \left. \left. + \frac{1}{2} h^2 u_x^2 - \frac{1}{3} h^2 (u_{xt} + uu_{xx}) \right) \right) = 0, \end{aligned} \quad (4c)$$

$$\begin{aligned} \partial_t \left(u - hh_x u_x - \frac{1}{3} h^2 u_{xx} \right) + \partial_x \left(gh + \frac{1}{2} u^2 - hh_x uu_x \right. \\ \left. - \frac{1}{2} h^2 u_x^2 - \frac{1}{3} h^2 uu_{xx} \right) = 0. \end{aligned} \quad (4d)$$

Eq. (4a) corresponds to conservation of mass, (4b) corresponds to conservation of momentum, (4c) corresponds to conservation of energy, and (4d) corresponds to conservation of irrotationality.

The Serre equations are invariant under the following transformation

$$h(x, t) = \hat{h}(x - st, t), \quad (5a)$$

$$u(x, t) = s + \hat{u}(x - st, t), \quad (5b)$$

$$\hat{x} = x - st, \quad (5c)$$

where s is a free parameter. This transformation physically represents adding a constant horizontal velocity s to the entire system. We choose this constant to be the velocity of propagation of the wave train of permanent form, c , which according to Stokes' second definition of wave celerity [30], corresponds to the uniform current that one has to add to suppress the horizontal momentum of the fluid.

El et al. [31] show that the Serre equations admit the following family of solutions

$$h(x, t) = a_0 + a_1 \text{dn}^2(\kappa(x - ct), k), \quad (6a)$$

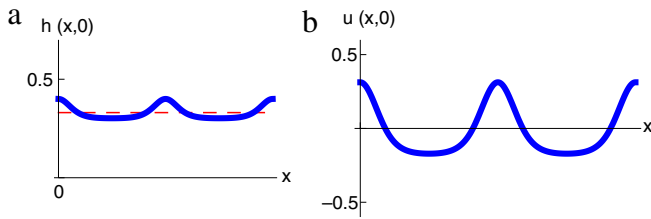


Fig. 2. Plots of the water depth, h , and depth-averaged horizontal velocity, u , corresponding to the solution given in Eq. (6) with $k = 0.99$, $a_0 = 0.3$ and $a_1 = 0.1$ at $t = 0$. The dashed line in (a) represents the mean water depth, h_0 .

$$u(x, t) = c \left(1 - \frac{h_0}{h(x, t)} \right), \quad (6b)$$

$$\kappa = \frac{\sqrt{3a_1}}{2\sqrt{a_0(a_0 + a_1)(a_0 + (1 - k^2)a_1)}}, \quad (6c)$$

$$c = \frac{\sqrt{ga_0(a_0 + a_1)(a_0 + (1 - k^2)a_1)}}{h_0}, \quad (6d)$$

where $k \in [0, 1]$, $a_0 > 0$ and $a_1 > 0$ are real parameters. This family of solutions to the Serre equations is the periodic generalization of the Rayleigh solitary wave solution (see Eq. (9)). It can be found by using the Jacobi elliptic function expansion method of Liu et al. [32]. In Eq. (6), $\text{dn}(\cdot, k)$ is a Jacobi elliptic function with elliptic modulus k . Byrd and Friedman [33] provide a thorough review of Jacobi elliptic functions and their properties. If $k \in (0, 1)$, the solutions given in Eq. (6) are spatially periodic with wavelength $\lambda = 2K(k)/\kappa$. The mean water depth, h_0 , is computed by averaging the water depth over one wavelength

$$h_0 = \frac{1}{\lambda} \int_0^\lambda h(x, t) dx = a_0 + a_1 \frac{E(k)}{K(k)}, \quad (7)$$

where $K(k)$ and $E(k)$ are the complete elliptic integrals of the first and second kinds, respectively [33]. Hence, the cnoidal solution of the Serre system is completely determined by fixing the numerical values for the parameters a_0 , a_1 and k . Fig. 2 contains representative plots of h and u versus x .

The solutions given in Eq. (6) are periodic if $k \in (0, 1)$. However, as $k \rightarrow 0^+$, these solutions limit to the following constant solution

$$h(x, t) = a_0 + a_1, \quad (8a)$$

$$u(x, t) = 0. \quad (8b)$$

In other words, as $k \rightarrow 0^+$, the solutions given in Eq. (6) limit to the trivial solution of a zero-velocity fluid with a horizontal surface at $a_0 + a_1$.

As $k \rightarrow 1^-$, the family of periodic solutions limits to the following two-parameter family of solitary wave solutions

$$h(x, t) = a_0 + a_1 \text{sech}^2(\kappa(x - ct)), \quad (9a)$$

$$u(x, t) = c \left(1 - \frac{a_0}{h(x, t)} \right), \quad (9b)$$

$$\kappa = \frac{\sqrt{3a_1}}{2a_0\sqrt{a_0 + a_1}}, \quad (9c)$$

$$c = \sqrt{g(a_0 + a_1)}. \quad (9d)$$

This family of solutions is known as the Rayleigh solitary wave solution.

In engineering practice, wave properties are often defined by wave height, H , wave period, T , and mean water depth, h_0 . The dispersion relation provides a link between celerity and spatial and temporal wave scales

$$c = \frac{\hat{\omega}}{\hat{k}}, \quad (10)$$

where $\hat{\omega} = 2\pi/T$ is the angular frequency and $\hat{k} = 2\pi/\lambda$ is the wave number. Using Eqs. (6)–(7) and previous definitions, it is possible to find the cnoidal solution of the Serre system for given H , T and h_0 by solving the following set of equations,

$$a_1 = \frac{H}{k^2}, \quad (11a)$$

$$a_0 = h_0 - a_1 \frac{E(k)}{K(k)}, \quad (11b)$$

$$\hat{\omega}^2 = \frac{3\pi^2 g a_1}{4[a_0 K(k) + a_1 E(k)]^2}, \quad (11c)$$

for a_0 , a_1 and k . This is done in the next section where solutions of the Serre system are compared with numerical and experimental results.

The horizontal, U , and vertical, W , components of water-particle velocities at any location (x, z) in the vertical plane are defined by the following expressions [20]

$$U(x, z, t) = u + \left(\frac{h^2}{6} - \frac{z^2}{2} \right) u_{xx}, \quad (12a)$$

$$W(x, z, t) = -zu_x, \quad (12b)$$

where z is the water depth measured from the bottom.

3. Kinematic properties of solitary and cnoidal waves

In this section we assess the accuracy and relevance of the closed-form solutions presented in the previous section. We compare predictions obtained from the solutions with measurements obtained from physical experiments. In particular, we compare free surface profiles and internal wave kinematics.

For solitary waves up to the breaking limit, comparisons are performed with the numerical solution of Tanaka [34] which is extremely accurate up to the highest solitary wave [35,36]. For periodic waves, comparisons are performed using the Stream Function Theory of Dean [37]. The experimental velocity profiles of LeMéhauté et al. [38] are also used to investigate the performance of the periodic solutions. For all cases, results obtained from the KdV equation are also presented. The KdV solutions are computed following the practical implementation proposed by Wiegel [39].

3.1. The kinematics of solitary waves

In this section, we consider the propagation of solitary waves over a quiescent fluid of constant depth. We focus on wave conditions which are beyond the range of validity of the classical Boussinesq or KdV equations. The numerical solution of Tanaka [34] is used for verification. We also present results from the KdV equation for comparison.

We first consider the results for a highly nonlinear solitary wave of height $H = 0.65$ m propagating over a quiescent water depth $h_0 = 1$ m. In this case, the nonlinear parameter is $\epsilon = 0.65$ which is far beyond the weak nonlinearity limit requiring $\epsilon \ll 1$. Free surface profiles computed from Tanaka, KdV and Serre are presented in Fig. 3(a). The Serre solitary wave profile is less “peaky” than the Tanaka solitary wave profile. Thus, the Serre model produces an overestimation of the water depth. This difference was noticed by Gobbi et al. [35] by comparing the Tanaka solution to several families of the Green–Naghdi (Serre) equations. Surprisingly, the weakly nonlinear solution provided by the classical KdV theory is better than Serre solution in describing the free surface profile. However, the situation is different when other wave properties are considered. Fig. 3(b) contains a plot of the horizontal velocity profile under the solitary wave crest as

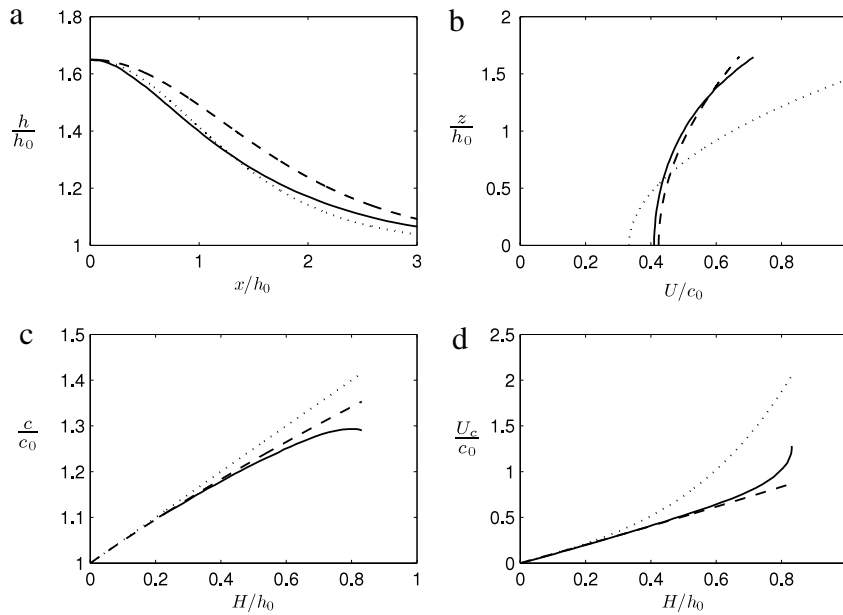


Fig. 3. Comparison between the Tanaka solitary wave solution (solid curves), KdV theory (dotted curves) and Serre theory (dashed curves). (a) Free surface profile for $H/h_0 = 0.65$, (b) horizontal velocity profile under wave crest for $H/h_0 = 0.65$, (c) wave celerity, and (d) horizontal velocity evaluated at the crest.

predicted by Serre's theory (Eq. (12a)), Tanaka and KdV. Results computed from the Serre equations are much closer to the Tanaka results than the KdV predictions. In fact, the KdV predictions deviate significantly from the Tanaka theory. This highlights the importance of using a fully nonlinear model to describe internal wave kinematics for large amplitude waves.

Fig. 3(c), (d) contain plots of the wave celerity and wave crest velocity nondimensionalized by the linear wave celerity, $c_0 = \sqrt{gh_0}$, for different values of the relative amplitude, H/h_0 , up to the highest possible solitary wave ($H/h_0 \simeq 0.83$). The wave celerity is computed for Serre's theory using Eq. (9d). The KdV theory provides good predictions for these quantities as long as $H/h_0 < 0.2$, but deviates more and more as the relative amplitude increases beyond 0.2. In particular, the KdV crest velocity prediction is rather poor for high amplitude solitary waves and results in large overestimations. Wave celerity and crest velocity estimates obtained from the Serre theory are in very good agreement with the Tanaka solution for $H/h_0 < 0.5$. This confirms the practical improvement in terms of kinematic properties produced by the Serre theory over the classical Boussinesq or KdV predictions. It is worth noting that crest velocity predictions obtained from the Serre equations are in good agreement with the Tanaka prediction up to relative amplitudes as high as $H/h_0 \simeq 0.7$ (which are considered to be nearly breaking).

3.2. The kinematics of periodic waves

In this subsection we investigate the performance of Serre and KdV cnoidal wave solutions in terms of several important kinematic properties. In order to assess wave celerity predictions, we use the accurate numerical results of Dean's [37] Stream Function Theory (SFT) as reference. The laboratory results of LeMéhauté et al. [38] are used to test the model predictions of velocity profiles under periodic waves.

Fig. 4 contains plots of wave celerity for different relative amplitudes versus the Ursell number. For moderately nonlinear waves (i.e. $H/h_0 \leq 0.2$), Fig. 4 shows that both the KdV and Serre theories agree with SFT-computed wave celerities over the whole range of Ursell numbers ($U_r > 1$). However, for higher relative amplitudes, the KdV theory systematically overestimates the wave

celerity for all investigated values of the Ursell number. This establishes that the KdV equation does not accurately represent the kinematics of strongly nonlinear, periodic, long waves. This fact corroborates the results for solitary waves discussed in Section 3.1 and evidences how the weakly nonlinear hypothesis embedded in the KdV model limits the application of the KdV theory. By comparison, the Serre cnoidal wave theory provides better agreement with the SFT-computed celerities for the whole range of investigated Ursell values up to a relative amplitude of $H/h_0 = 0.5$.

It is important to note that the wave celerity is overestimated by the KdV theory for highly nonlinear waves ($H/h_0 > 0.2$) over the whole range of Ursell numbers, while the Serre theory produces an underestimation of the wave celerity for $H/h_0 > 0.5$ over a limited range of Ursell numbers (i.e. $U_r \sim O(1-100)$). Thus, wave celerity estimated from the Serre cnoidal theory asymptotically converges to the nonlinear long wave (nondispersive) limit as $U_r \gg 1$ while KdV theory does not.

As a last verification, we consider experimental measurements of velocity profiles under crests of periodic waves performed by LeMéhauté et al. [38]. They investigated several waves with $H/h_0 \sim 0.4-0.5$ propagating over a horizontal bottom. Comparisons between measured values and values predicted by the KdV and Serre cnoidal theories are included in Fig. 5. In general, the predictions obtained from the Serre system are in better agreement with the physical measurements than predictions obtained from KdV, except for the $H/h_0 = 0.389$, $T\sqrt{g/h_0} = 22.49$ case. In this case, the experimental data is spread between the two theoretical predictions. For the largest and longest wave (Fig. 5(c)), only minor differences between Serre's velocity profile and measurements are observed near the free surface. Nevertheless, the agreement is fair and confirms the relevance of Serre theory in predicting internal kinematic properties of nonlinear shallow water waves.

4. Linear stability

In order to study the linear stability of the solutions given in Eq. (6), we enter a coordinate frame moving with the velocity of the waves via the following transformation

$$\chi = x - ct, \tag{13a}$$

$$\tau = t, \tag{13b}$$

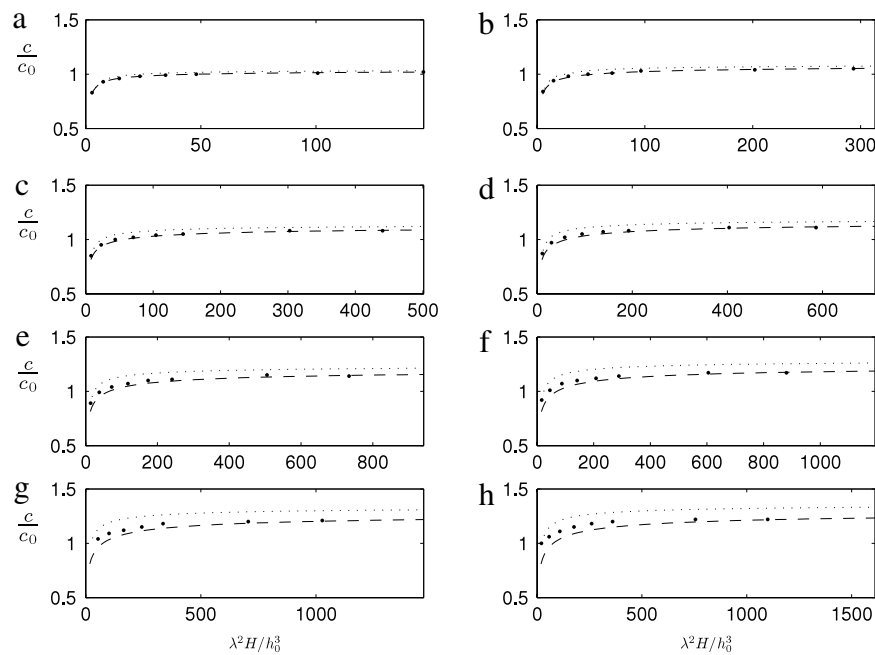


Fig. 4. Comparisons of wave celerity for periodic waves obtained from Dean's Stream Function Theory (diamonds), KdV cnoidal wave theory (dotted curves), and Serre cnoidal wave theory (dashed curves) for different values of the Ursell number and relative amplitudes. (a) $H/h_0 = 0.1$, (b) $H/h_0 = 0.2$, (c) $H/h_0 = 0.3$, (d) $H/h_0 = 0.4$, (e) $H/h_0 = 0.5$, (f) $H/h_0 = 0.6$, (g) $H/h_0 = 0.7$, (h) $H/h_0 = 0.75$.

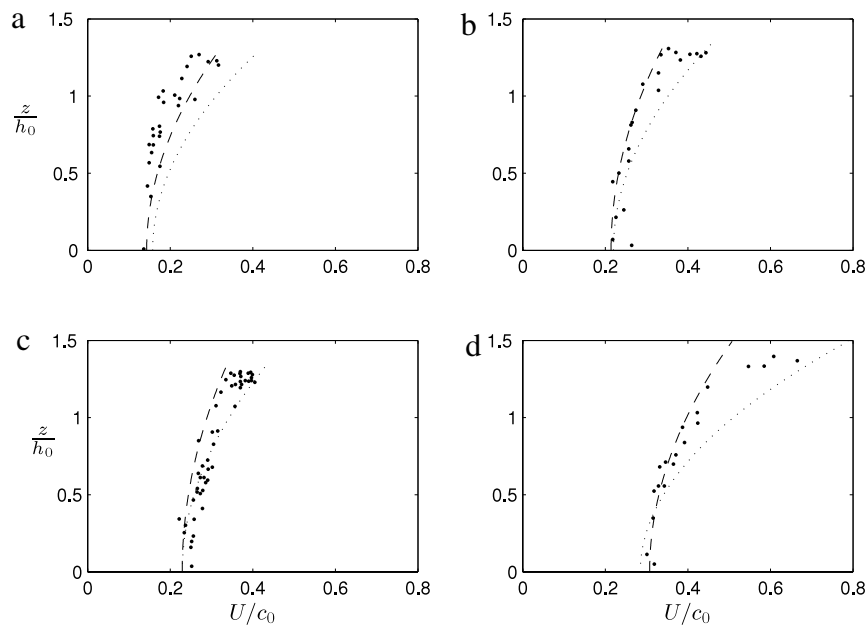


Fig. 5. Horizontal velocity profiles under crests of periodic waves for different parameter values. Experimental measurements (bold dots), KdV cnoidal theory (dotted curves) and Serre cnoidal theory (dashed curves). (a) $H/h_0 = 0.434$, $T\sqrt{g/h_0} = 8.59$, (b) $H/h_0 = 0.420$, $T\sqrt{g/h_0} = 15.86$, (c) $H/h_0 = 0.389$, $T\sqrt{g/h_0} = 22.49$, and (d) $H/h_0 = 0.548$, $T\sqrt{g/h_0} = 27.26$.

where c is defined in Eq. (6d). After this change of variables, the Serre equations are

$$h_\tau - ch_\chi + (hu)_\chi = 0, \tag{14a}$$

$$u_\tau - cu_\chi + uu_\chi + gh_\chi$$

$$- \frac{1}{3h} (h^3 (u_{\chi\tau} - cu_{\chi\chi} + uu_{\chi\chi} - (u_\chi)^2))_\chi = 0, \tag{14b}$$

and the solutions given in Eq. (6) simplify to the following time-independent solutions

$$h = \eta_0(\chi) = a_0 + a_1 \text{dn}^2(\kappa\chi, k), \tag{15a}$$

$$u = u_0(\chi) = c \left(1 - \frac{h_0}{h(\chi)} \right), \tag{15b}$$

where κ , c , and h_0 are defined in Eqs. (6c), (6d) and (7), respectively.

We consider perturbed solutions of the form

$$h_{\text{pert}}(\chi, \tau) = \eta_0(\chi) + \mu\eta_1(\chi, \tau) + \mathcal{O}(\mu^2), \tag{16a}$$

$$u_{\text{pert}}(\chi, \tau) = u_0(\chi) + \mu u_1(\chi, \tau) + \mathcal{O}(\mu^2), \tag{16b}$$

where η_1 and u_1 are real-valued functions and μ is a small real parameter. Substituting Eq. (16) into Eq. (14) and linearizing leads

to a pair of coupled, linear partial differential equations that are constant coefficient in τ . Without loss of generality, assume

$$\eta_1(\chi, \tau) = H(\chi)e^{\Omega\tau} + c.c., \tag{17a}$$

$$u_1(\chi, \tau) = U(\chi)e^{\Omega\tau} + c.c., \tag{17b}$$

where $H(\chi)$ and $U(\chi)$ are complex-valued functions, Ω is a complex constant, and $c.c.$ denotes complex conjugate. If Ω has a positive real part, then the perturbations η_1 and u_1 grow exponentially in τ and the solution is said to be linearly unstable. Further, if the real part of Ω , $\Re(\Omega)$, is positive, we define it to be the growth rate of the perturbation.

Substituting (17) into the linearized system of PDEs gives

$$\mathcal{L} \begin{pmatrix} H \\ U \end{pmatrix} = \Omega \mathcal{M} \begin{pmatrix} H \\ U \end{pmatrix}, \tag{18}$$

where \mathcal{L} and \mathcal{M} are the linear differential operators defined by

$$\mathcal{L} = \begin{pmatrix} -u'_0 + (c - u_0)\partial_\chi & -\eta'_0 - \eta_0\partial_\chi \\ \mathcal{L}_{21} & \mathcal{L}_{22} \end{pmatrix}, \tag{19a}$$

$$\mathcal{M} = \begin{pmatrix} 1 & 0 \\ 0 & 1 - \eta_0\eta'_0\partial_\chi - \frac{1}{3}\eta_0^2\partial_{\chi\chi} \end{pmatrix}, \tag{19b}$$

where prime represents derivative with respect to χ and

$$\begin{aligned} \mathcal{L}_{21} = & -\eta'_0(u'_0)^2 - c\eta'_0u''_0 - \frac{2}{3}c\eta_0u'''_0 + \eta'_0u_0u''_0 \\ & - \frac{2}{3}\eta_0u'_0u''_0 + \frac{2}{3}\eta_0u_0u'''_0 \\ & + (\eta_0u_0u''_0 - g - \eta_0(u'_0)^2 - c\eta_0u''_0)\partial_\chi, \end{aligned} \tag{20a}$$

$$\begin{aligned} \mathcal{L}_{22} = & -u'_0 + \eta_0\eta'_0u''_0 + \frac{1}{3}\eta_0^2u'''_0 \\ & + \left(c - u_0 - 2\eta_0\eta'_0u'_0 - \frac{1}{3}\eta_0^2u''_0 \right) \partial_\chi \\ & + \left(\eta_0\eta'_0u_0 - c\eta_0\eta'_0 - \frac{1}{3}\eta_0^2u'_0 \right) \partial_{\chi\chi} \\ & + \left(\frac{1}{3}\eta_0^2u_0 - \frac{1}{3}c\eta_0^2 \right) \partial_{\chi\chi\chi}. \end{aligned} \tag{20b}$$

The system given in Eq. (18), subject to periodic boundary conditions, is a differential eigenvalue problem. The eigenvalues, Ω s, determine how the perturbations evolve in τ . The corresponding eigenfunctions, H and U , determine the χ structure of the perturbations.

In order to find approximations to the eigenvalues and eigenfunctions corresponding to the solutions given in Eq. (15), we employ the Fourier-Floquet-Hill (FFH) method of Deconinck and Kutz [40]. This numerical method is spectrally accurate for differential eigenvalue problems with periodic coefficients (such as the one under consideration here) and allows the computation of eigenfunctions of the form

$$\begin{pmatrix} H \\ U \end{pmatrix} = e^{i\rho\chi} \begin{pmatrix} H^p \\ U^p \end{pmatrix}, \tag{21}$$

where H^p and U^p are periodic in χ with period $2K/\kappa$ and $\rho \in [-\pi\kappa/(4K), \pi\kappa/(4K))$. Therefore, if $\rho = 0$, then the perturbation has the same period as the unperturbed solution. If the unperturbed solution is periodic, then all bounded eigenfunctions of (18) have the form given in Eq. (21) [41,42,40].

In the remainder of this section, we present results from numerical simulations. The spectral plots focus on regions where $\Re(\Omega) > 0$ because these are the regions that establish instability. Further, the Hamiltonian structure of the system [24] establishes that the second, third, and fourth quadrants of the complex- Ω plane are reflections of the first quadrant. We also include a plots of three unstable eigenfunctions in Fig. 8.

Table 1

The values of a_1 , δ , ϵ , Λ and U_f for Case I numerical simulations.

Case I				
a_1	δ	ϵ	Λ	U_f
0.05	0.0922	0.0840	0.0077	9.893
0.1	0.1302	0.1524	0.0198	8.995
0.2	0.1841	0.2568	0.0473	7.579
0.3	0.2258	0.3328	0.0751	6.526

4.1. Case I: fixed a_0 and k

For this series of numerical simulations, $a_0 = 0.3$ and $k = 0.75$ were fixed while a_1 was varied. Changing the value of a_1 changes the amplitude and the period of the solution. As a_1 increases, δ , ϵ and Λ all increase. The values of the parameters for these simulations are included in Table 1. Fig. 6 contains plots of spectra obtained using the FFH method with 100 positive Fourier modes (a measure of spectral resolution) and 5000 different ρ values (a measure of the number of different quasi-periods examined).

Observations:

- If a_1 is small enough, there are no Ω s with positive real part and therefore the solution is linearly stable. This establishes that (in this parameter regime) waves with sufficiently small amplitude are stable.
- If a_1 is large enough, then there are Ω s with positive real part and therefore the solution is linearly unstable. This establishes that waves with sufficiently large amplitude are unstable.
- The cutoff between stability and instability occurs at $a_1 \approx 0.023$.
- The maximum growth rate increases as a_1 increases.
- All instabilities are oscillatory instabilities. That is, every Ω that has a positive real part has a nonzero imaginary part.
- The rate of instability oscillation, $\Im(\Omega)$, (the imaginary part of Ω) increases as a_1 increases.
- For these parameter values, there is only one band of instabilities for each value of a_1 . In the first quadrant, each of these bands is similar in shape to a half oval.
- Generally, the instability with maximal growth rate corresponds to a perturbation with nonzero ρ . This means that the period of the most unstable mode is longer than that of the unperturbed solution.

4.2. Case II: fixed a_0 and a_1

For this series of numerical simulations, $a_0 = 0.3$ and $a_1 = 0.1$ were fixed while k was varied. Changing the parameter k changes the amplitude, period and steepness of the wave. As k increases, ϵ increases, δ decreases, and Λ increases up to $k \approx 0.925$ and then decreases. The values of ϵ , δ , Λ and U_f corresponding to Case II numerical simulations are included in Table 2. Fig. 7 contains plots of spectra obtained using the FFH method with 100 positive Fourier modes and 10,000 ρ values. (Increasing the number of Fourier modes used did not qualitatively change the plots.)

Observations:

- If k is small enough, there is no instability. If k is large enough, there is instability. This establishes that waves with sufficiently small steepness/amplitude are stable and that waves with sufficiently large steepness/amplitude are unstable.
- The cutoff between stability and instability occurs at $k \approx 0.30$.
- Each of the bands in the first quadrant is similar in shape to a compressed half oval. As k increases, the number of bands of instability increases.
- All instabilities are oscillatory instabilities.

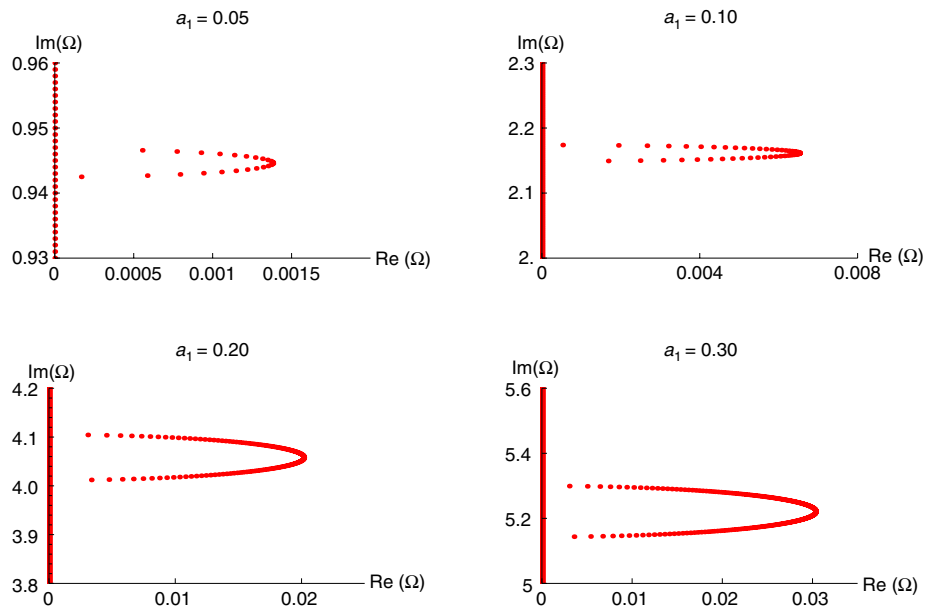


Fig. 6. Results from Case I numerical simulations. Discrete representations of the spectra of (18) corresponding to $a_0 = 0.3$, $k = 0.75$ and four different values of a_1 .

Table 2
The values of k , δ , ϵ , Λ and U_r for Case II numerical simulations.

Case II				
k	δ	ϵ	Λ	U_r
0.5	0.1482	0.0646	0.0096	2.941
0.9	0.1078	0.2306	0.0249	19.825
0.99	0.0708	0.2964	0.0210	59.044
0.999	0.0517	0.3096	0.0160	115.71

Table 3
The values of k , δ , ϵ , Λ and U_r for Case III numerical simulations.

Case III				
k	δ	ϵ	Λ	U_r
0.5	0.2967	0.1542	0.0458	1.753
0.9	0.1196	0.2752	0.0329	19.233
0.99	0.0715	0.3018	0.0216	59.018
0.999	0.0518	0.3102	0.0161	115.72

- As k increases away from zero, the maximum growth rate increases until $k \approx 0.947$. Above this value, the maximum growth rate decreases. At $k = 0.947$, the maximum growth rate is 0.0132.
- Generally, the instability with maximal growth rate is a $\rho \neq 0$ perturbation.

Fig. 8 contains plots of a representative sampling of H^P and U^P corresponding to an unperturbed solution with $a_0 = 0.3$, $a_1 = 0.1$ and $k = 0.99$ (i.e. the solution shown in Fig. 2). They are plotted on an interval twice the length of the period of the unperturbed solution. For clarity, the effect of the exponential factor of the eigenfunction, $\exp(i\rho\chi)$ (see Eq. (21)) is not included. In order to obtain the complete eigenfunctions, one must multiply the functions shown in Fig. 8 by $\exp(i\rho\chi)$. Fig. 8(i) and (ii) contain plots of the components of the most unstable mode ($\Omega = 0.0104 + 0.6939i$, $\rho = -0.1923$). Fig. 8(iii) and (iv) contain plots of H^P and U^P corresponding to ($\Omega = 0.0095 + 2.1765i$, $\rho = 0.0688$). Fig. 8(v) and (vi) contain plots of H^P and U^P corresponding to ($\Omega = 0.0039 + 4.7322i$, $\rho = 0.0148$).

Observations:

- The H^P and U^P shown in Fig. 8 correspond to quasi-periodic eigenfunctions because $\rho \neq 0$.
- The given H^P and U^P correspond to unstable eigenfunctions because $\Re(\Omega) > 0$.
- For a given band of eigenvalues, H^P and U^P have a fixed number of oscillations. Changing ρ while remaining in the same band changes the value of the eigenvalue and the shapes of H^P and U^P , but not the number of oscillations.
- Bands of eigenvalues with larger values of $\Im(\Omega)$ correspond to more oscillatory H^P and U^P .

4.3. Case III: fixed a_0 and wave amplitude

For this series of numerical simulations, a_0 and the wave height, $a_1 k^2$, were fixed at 0.3 and 0.1, respectively. The parameters k and a_1 were varied simultaneously in order to ensure that the wave height remained fixed. Changes of this sort modify the period and the steepness of the solution simultaneously. The values of the corresponding δ , ϵ , Λ and U_r are included in Table 3. Fig. 9 contains plots of spectra obtained using the FFH method with 100 positive Fourier modes and 10,000 ρ values.

Observations:

- If k is small enough, there is no instability. If k is large enough, there is instability. This establishes that waves with sufficiently small steepness/amplitude are stable and that waves with sufficiently large steepness/amplitude are unstable.
- The cutoff between stability and instability occurs at $k \approx 0.102$.
- Each of the bands in the first quadrant is similar in shape to a compressed half oval. As k increases, the number of bands of instabilities increases.
- All instabilities are oscillatory.
- As k increases away from zero, the maximum growth rate increases until $k \approx 0.86$. Above this value, the maximum growth rate decreases. At $k = 0.86$, the maximum growth rate is 0.020.
- Generally, the instability with maximal growth rate is a $\rho \neq 0$ perturbation.

Note that in all sets of simulations, as $k \rightarrow 0$, $\Re(\Omega) \rightarrow 0$. This is consistent with the fact that $k = 0$ corresponds to a stationary fluid with flat surface.

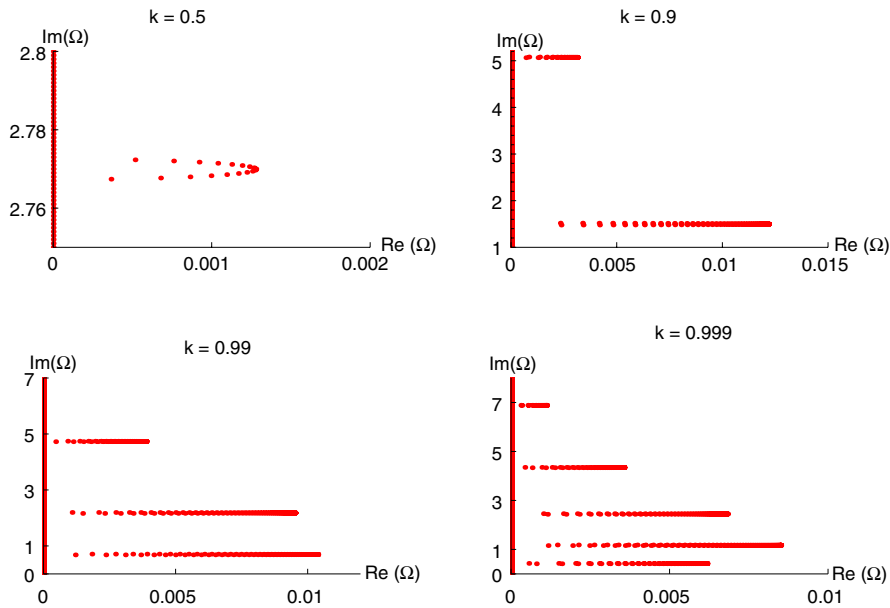


Fig. 7. Results from Case II numerical simulations. Discrete representations of the spectra of (18) corresponding to $a_0 = 0.3$, $a_1 = 0.1$ and four different values of k .

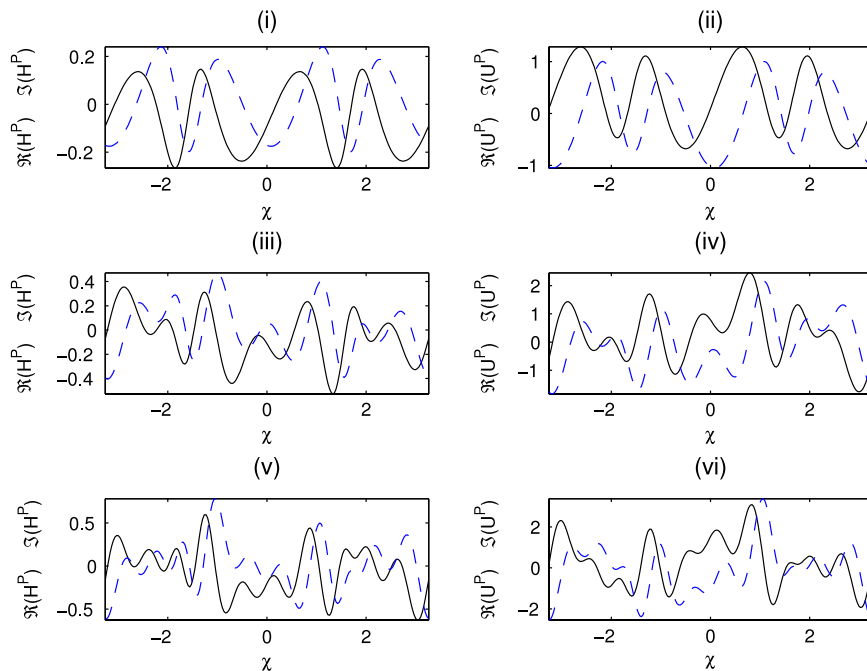


Fig. 8. Plots of H^P and U^P corresponding to $a_0 = 0.3$, $a_1 = 0.1$ and $k = 0.99$. The solid and dashed curves correspond to the real and imaginary parts, respectively. (i) and (ii) $\Omega = 0.0104 + 0.6939i$, $\rho = -0.1923$. (iii) and (iv) $\Omega = 0.0095 + 2.1765i$, $\rho = 0.0688$. (v) and (vi) $\Omega = 0.0039 + 4.7322i$, $\rho = 0.0148$.

All of the instabilities presented herein have relatively small growth rates. These instabilities may not be physically observable due to dissipative or other physical effects because such effects may overwhelm any growth. Further, as k becomes very close to 1, the instability growth rate decreases (possibly to zero). If the growth rate decreases to zero in the solitary wave limit, the numerical results would corroborate Li's stability result [23,24]. This may also explain the apparently stable Serre solitary waves created by Guizien and Barthélemy [28].

Finally, the results from our numerical simulations are consistent with the recent results of Deconinck and Oliveras [43] where they study the stability of periodic solutions of the Ablowitz et al. [44] formulation of the Euler equations and obtain spectra similar to those in Figs. 6–9.

5. Summary

Several interesting properties of the system of nonlinear partial differential equations known as Serre equations were investigated in this article. This fully nonlinear set of Boussinesq-type equations admits a closed-form three-parameter family of periodic solutions that describe shallow water wave propagation on horizontal bottoms. These solutions limit to the Rayleigh solitary wave solution as $k \rightarrow 1^-$ and to the trivial case of a fluid at rest when $k \rightarrow 0^+$. Comparisons between accurate numerical solutions and experimental measurements have shown that the cnoidal and solitary wave solutions of the Serre equations perform much better than KdV solutions in describing the kinematics of highly nonlinear waves propagating in shallow waters.

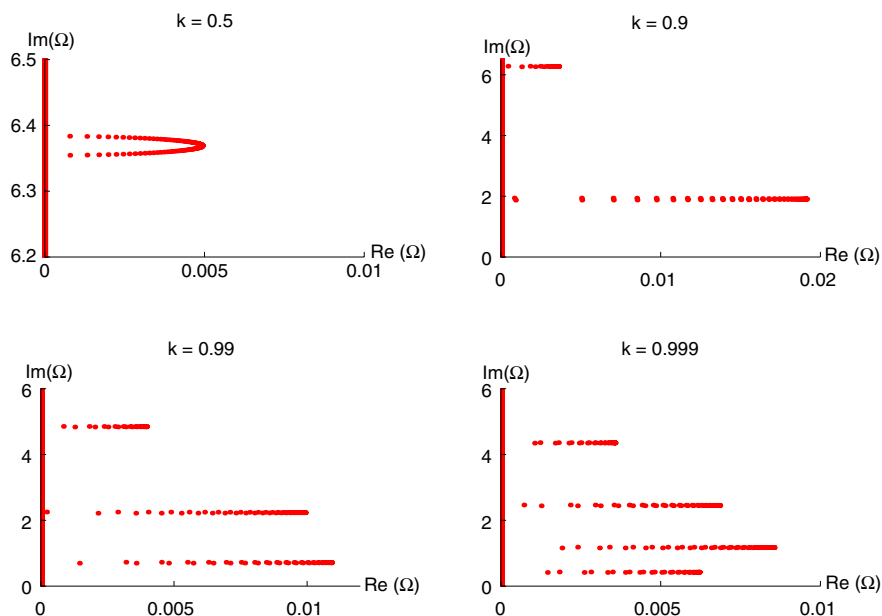


Fig. 9. Results from Case III numerical simulations. Discrete representations of the spectra of (18) corresponding to $a_1 k^2 = 0.1$, $a_0 = 0.3$ and four different values of k .

We studied the stability of these solutions for a variety of parameter values, while respecting their meaningful physical range. Spectral plots indicate that waves of small amplitude/steepness are stable while waves with sufficiently large amplitude/steepness are unstable.

Acknowledgements

This work was accomplished during a sabbatical leave of Professor John D. Carter at the Departamento de Ingeniería Hidráulica y Ambiental, Pontificia Universidad Católica de Chile (PUC). Financial support from the School of Engineering (PUC) and ECOS-Conicyt research grant No C07U01 are gratefully acknowledged.

References

[1] P.A. Madsen, H.A. Schäffer, Higher-order Boussinesq-type equations for surface gravity waves: derivation and analysis, *Phil. Trans. R. Soc. Lond. Ser. A* 356 (1998) 3123–3184.
 [2] J. Boussinesq, Théorie des ondes et des remous qui se propagent le long d'un canal rectangulaire horizontal, en communiquant au liquide contenu dans ce canal des vitesses sensiblement pareilles de la surface au fond, *J. Math. Pures Appl.* 2 (1872) 55–108.
 [3] A.J.-C.B. Saint-Venant, Théorie du mouvement non-permanent des eaux avec application aux crues des rivières et à l'introduction des marées dans leur lit, *C. R. Acad. Sci. Paris* 73 (1871) 147–154.
 [4] D.J. Korteweg, D. de Vries, On the change of form of long waves advancing in a rectangular canal, and on a new type of long stationary wave, *Phil. Mag.* 39 (1895) 422–443.
 [5] F. Serre, Contribution à l'étude des écoulements permanents et variables dans les canaux, *Houille Blanche* 8 (1953) 374–388.
 [6] H. Jeffrey, B.S. Jeffrey, *Methods of Mathematical Physics*, Cambridge University Press, 1946.
 [7] R.M. Miura, Korteweg–de Vries equation and generalizations I. A remarkable explicit nonlinear transformation, *J. Math. Phys.* 9 (1968) 1202–1204.
 [8] J.W. Miles, The Korteweg–de Vries equation, a historical essay, *J. Fluid Mech.* 106 (1981) 131–147.
 [9] M.J. Ablowitz, H. Segur, *Solitons and the Inverse Scattering Transform*, SIAM, Philadelphia, 1981.
 [10] J.S. Russell, Report on waves, in: Report of the Fourteenth Meeting of the British Association for the Advancement of Science, York, 1844, pp. 311–390.
 [11] N.J. Zabusky, C.J. Galvin, Shallow-water waves, the Korteweg–de Vries equation and solitons, *J. Fluid Mech.* 47 (1971) 811–824.
 [12] J.L. Hammack, H. Segur, The Korteweg–de Vries equation and water waves. Part 2. Comparison with experiments, *J. Fluid Mech.* 65 (1974) 289–314.
 [13] T.B. Benjamin, The stability of solitary waves, *Proc. R. Soc. Lond. Ser. A* 328 (1972) 153–183.

[14] N. Bottman, B. Deconinck, KdV cnoidal waves are linearly stable, *Discrete Contin. Dyn. Syst. A* 25 (2009) 1163–1180.
 [15] J.L. Bona, M. Chen, J.-C. Saut, Boussinesq equations and other systems for small-amplitude long waves in nonlinear dispersive media. I: derivation and linear theory, *J. Nonlinear Sci.* 12 (2002) 283–318.
 [16] M. Chen, C.W. Curtis, B. Deconinck, C.W. Lee, N. Nguyen, Spectral stability of stationary solutions of a Boussinesq system describing long waves in dispersive media, *SIAM J. Appl. Dyn. Syst.* 9 (2010) 999–1018.
 [17] F. Serre, Contribution à l'étude des écoulements permanents et variables dans les canaux, *Houille Blanche* 8 (1953) 830–872.
 [18] C.H. Su, C.S. Gardner, KdV equation and generalizations. Part III. Derivation of Korteweg–de Vries equation and Burgers equation, *J. Math. Phys.* 10(3) (1969) 536–539.
 [19] A.E. Green, P.M. Naghdi, A derivation of equations for wave propagation in water of variable depth, *J. Fluid Mech.* 78 (1976) 237–246.
 [20] E. Barthélemy, Nonlinear shallow water theories for coastal waves, *Surv. Geophys.* 25 (2004) 315–337.
 [21] R. Cienfuegos, E. Barthélemy, P. Bonneton, A fourth-order compact finite volume scheme for fully nonlinear and weakly dispersive Boussinesq-type equations. Part I: model development and analysis, *Internat. J. Numer. Methods Fluids* 51 (2006) 1217–1253.
 [22] F. Dias, P. Milewski, On the fully-nonlinear shallow-water generalized Serre equations, *Phys. Lett. A* 374 (2010) 1049–1053.
 [23] Y.A. Li, Linear stability of solitary waves of the Green–Naghdi equations, *Commun. Pure Appl. Math.* LIV (2001) 0501–0536.
 [24] Y.A. Li, Hamiltonian structure and linear stability of solitary waves of the Green–Naghdi equations, *J. Nonlinear Math. Phys.* 9 (2002) 99–105.
 [25] F.J. Seabra-Santos, D.P. Renouard, A.M. Temperville, Numerical and experimental study of the transformation of a solitary wave over a shelf or isolated obstacle, *J. Fluid Mech.* 176 (1987) 117–134.
 [26] R. Cienfuegos, E. Barthélemy, P. Bonneton, A fourth-order compact finite volume scheme for fully nonlinear and weakly dispersive Boussinesq-type equations. Part II: boundary conditions and validation, *Internat. J. Numer. Methods Fluids* 53 (2007) 1423–1455.
 [27] R. Cienfuegos, E. Barthélemy, P. Bonneton, Wave-breaking model for Boussinesq-type equations including roller effects in the mass conservation equation, *J. Waterway Port Coastal Ocean Engrg.* 136 (1) (2010) 10–26.
 [28] K. Guizien, E. Barthélemy, Accuracy of solitary wave generation by a piston wave maker, *J. Hydraul. Res.* 40 (3) (2002) 321–331.
 [29] D. Lannes, P. Bonneton, Derivation of asymptotic two-dimensional time-dependent equations for surface water wave propagation, *Phys. Fluids* 21 (1) (2009) 016601.
 [30] G.G. Stokes, On the theory of oscillatory waves, *Math. Phys. Papers* 1 (1880) 197–229.
 [31] G.A. El, R.H.J. Grimshaw, N.F. Smyth, Unsteady undular bores in fully nonlinear shallow-water theory, *Phys. Fluids* 18 (2006) 027104.
 [32] S. Liu, Z. Fu, S. Liu, Q. Zhao, Jacobi elliptic function expansion method and periodic wave solutions of nonlinear wave equations, *Phys. Lett. A* (2001) 69–74.
 [33] P.F. Byrd, M.D. Friedman, *Handbook of Elliptic Integrals for Scientists and Engineers*, Springer-Verlag, New York, 1971.
 [34] M. Tanaka, The stability of solitary waves, *Phys. Fluids* 29 (1986) 650–655.
 [35] M.F. Gobbi, J.T. Kirby, G. Wei, A fully nonlinear Boussinesq model for surface waves. Part 2. Extension to $O(kh)^4$, *J. Fluid Mech.* 405 (2000) 181–210.

- [36] P.A. Madsen, H.B. Bingham, H. Liu, A new Boussinesq method for fully nonlinear waves from shallow to deep water, *J. Fluid Mech.* 462 (2002) 1–30.
- [37] R.G. Dean, Stream function representation of nonlinear ocean waves, *J. Geophys. Res.* 70 (18) (1965) 4561–4572.
- [38] B. Le Méhauté, D. Divoky, A. Lin, Shallow water waves: a comparison of theories and experiments, in: *Proceedings of the 11th International Conference on Coastal Engineering*, London, United Kingdom, 1968, pp. 86–107.
- [39] R.L. Wiegel, A presentation of cnoidal wave theory for practical applications, *J. Fluid Mech.* 7 (2) (1960) 273–286.
- [40] B. Deconinck, J.N. Kutz, Computing spectra of linear operators using Hill's method, *J. Comput. Phys.* 219 (2006) 296–321.
- [41] G.W. Hill, On the part of the lunar perigee which is a function of the mean motion of the sun and the moon, *Acta Math.* 8 (1886) 1–36.
- [42] G. Floquet, Sur les équations différentielles linéaires à coefficients périodiques, *Ann. Sci. Éc. Norm. Supér.* 12 (2) (1883) 47–89.
- [43] B. Deconinck, K. Oliveras, The instability of periodic surface gravity waves, *J. Fluid Mech.* (2010) (in press).
- [44] M.J. Ablowitz, A.S. Fokas, Z.H. Musslimani, On a new non-local formulation of water waves, *J. Fluid Mech.* (2006).